# Application of a Two-Level Rolling Horizon Optimization Scheme to a Solid-Oxide Fuel Cell and Compressed Air Energy Storage Plant for the Optimal Supply of Zero-Emissions Peaking Power


### *Authors:*

Jake Nease, Nina Monteiro, Thomas A. Adams II



*Date Submitted:* 2018-06-19

*Keywords:* Compressed Air Energy Storage, Simulation, Aspen Plus, Rolling Horizon Optimization, Carbon Capture, Solid Oxide Fuel Cells, Optimization



*Abstract:*

We present a new two-level rolling horizon optimization framework applied to a zero-emissions coal-fueled solid-oxide fuel cell power plant with compressed air energy storage for peaking applications. Simulations are performed where the scaled hourly demand for the year 2014 from the Ontario, Canada market is met as closely as possible. It was found that the proposed two-level strategy, by slowly adjusting the SOFC stack power upstream of the storage section, can improve load-following performance by 86% compared to the single-level optimization method proposed previously. A performance analysis indicates that the proposed approach uses the available storage volume to almost its maximum potential, with little improvement possible without changing the system itself. Further improvement to load-following is possible by increasing storage volumes, but with diminishing returns. Using an economically-focused objective function can improve annual revenue generation by as much as 6.5%, but not without a significant drop-off in load-following performance.



*Record Type:* Postprint

*Submitted To:* LAPSE (Living Archive for Process Systems Engineering)

| | |
|---|---|
| *Citation (overall record, always the latest version):* | LAPSE:2018.0141 |
| *Citation (this specific file, latest version):* | LAPSE:2018.0141-1 |
| *Citation (this specific file, this version):* | LAPSE:2018.0141-1v1 |

*DOI of Published Version:* https://doi.org/10.1016/j.compchemeng.2016.08.004

*Embargoed Until:* 2018-08-21

# Application of a Two-Level Rolling Horizon Optimization Scheme to a Solid-Oxide Fuel Cell and Compressed Air Energy Storage Plant for the Optimal Supply of Zero-Emissions Peaking Power

*Jake Nease [a], Nina Monteiro [b], Thomas A. Adams II [a*]*

[a] Department of Chemical Engineering, McMaster University. 1280 Main Street West, Hamilton, Ontario, Canada

[b] Engenharia Química, Universidade Federal do Paraná. Avenida Coronel Francisco Heráclito dos Santos, Jardim das Américas, Curitiba, Brazil

* Corresponding author. 1280 Main Street West, Hamilton, Ontario, Canada, L8S 4L7. Tel.: +1 (905) 525-9140 x24782; E-mail address: tadams@mcmaster.ca

## Abstract

We present a new two-level rolling horizon optimization framework applied to a zero-emissions coal-fueled solid-oxide fuel cell power plant with compressed air energy storage for peaking applications. Simulations are performed where the scaled hourly demand for the year 2014 from the Ontario, Canada market is met as closely as possible. It was found that the proposed two-level strategy, by slowly adjusting the SOFC stack power upstream of the storage section, can improve load-following performance by 86% compared to the single-level optimization method proposed previously. A performance analysis indicates that the proposed approach uses the available storage volume to almost its maximum potential, with little improvement possible without changing the system itself. Further improvement to load-following is possible by increasing storage volumes, but with diminishing returns. Using an economically-focused objective function can improve annual revenue generation by as much as 6.5%, but not without a significant drop-off in load-following performance.

## 1. Introduction

Due to pressure from governmental regulations, the constant knowledge of waning resources, and the rapidly improving technologies for generating reliable electricity from renewable resources, classic power plants utilizing fossil fuels such as coal and natural gas (NG) are being eschewed in favour of more environmentally friendly alternatives, particularly in North America. In fact, it is projected that by 2035 the United States and Canada will each generate approximately 10% [1] and 16% [2] of their power from non-hydroelectric renewable resources, respectively. However, a current prohibitive feature of renewable resources is that they are typically intermittent in nature (variable and unpredictable wind/cloud patterns, day/night cycles, *etc.*), which makes them unsuitable for use in a bulk supply scenario, which requires high reliability and consistency. Although it is possible to use large-scale intermittent energy storage techniques such as pumped hydro storage [3], compressed air energy storage (CAES) [4], molten salt loops [5], material phase changes [6] and others in order to levelized the power supply from intermittent renewables, the high variability of renewables coupled with the limited capacity of energy storage techniques make

for significantly difficult planning and operability concerns. These problems are further exacerbated by the low capacities of renewables and round-trip efficiency losses in potential energy storage systems, both of which must be improved before renewable energy sources will be capable of fully displacing fossil fuel-based power.

While the paradigm in energy sources for electricity generation moves to renewables, the use of fossil fuels still constitutes a major portion of the power generated worldwide. In fact, it is estimated that the United States will still supply approximately 34% of its electricity demand through the consumption of coal [1]. Furthermore, at its current usage rate it is estimated that North America possesses sufficient reserves for over 250 years of domestic coal consumption [7]. This large supply of coal, combined with the forecasted importance of it as a future resource, provides an opportunity and challenge to use make the most efficient usage of this resource as possible.

Solid oxide fuel cells (SOFCs) can be used to generate reliable "peaking" electric power at the bulk scale with minimal environmental impact when appropriate carbon capture strategies are used [8]-[10]. To do this, SOFCs fueled by coal [11],[12] or natural gas (NG) [13] can be integrated with compressed air energy storage (CAES) in order to exploit some process synergies that enable the system to meet an ever-changing electricity demand through the day despite having no direct $CO_2$ emissions. The electric power can be generated at a competitive market price, even without government subsidies, once the SOFC technology reaches maturity. Furthermore, detailed life cycle analyses have shown that these proposed SOFC plants have significantly lower environmental impacts than other state of the art options such as the NG combined cycle (NGCC) [14] or supercritical pulverized coal (SCPC) [15] process.

In the SOFC/CAES system, the SOFCs produce power at a constant, steady rate, and the CAES system either stores or releases compressed air in different amounts that can change hourly or even more frequently. The goal is to adjust the amount stored or released throughout the day in order to change the total net electricity production needed to meet the demand. However, because the SOFC output is limited and the CAES storage capacity is finite, the power demand cannot always be met every hour of every day, week, and month. Therefore, an operating policy is required which must decide how well to match the production and demand at any given time. For example, the original proof-of-concept used a naïve (or "greedy") operating policy, which was to always store or release energy at any given moment such that power demand at that moment would be met exactly. Although this worked sometimes, it also led to significant "large misses" when the CAES storage volume reached minimum or maximum capacity, leading to all flexibility in the system being lost instantaneously [11]-[13]. The concept of real-time optimization [16]-[19] being used in chemical plants and even with small SOFC experimental setups [20] led to the eventual development of a rolling horizon optimization (RHO) technique that uses forecasts of future demand to optimally plan the next series of control moves based on the operating and storage constraints of the SOFC/CAES system [21]. With this approach, the system would predict a potential problem and then avoid it by scheduling a series of "small misses" over time in order to prevent a more serious large miss. Although this method improves the day-to-day performance and peak-following capability of the SOFC/CAES plant, it does not solve the problem of seasonal changes in demand, such as a generally higher demand (up to 30% more) during the summer and winter months compared to autumn and spring.

Therefore, to better solve this problem, we present a new, expanded version of the RHO concept by formulating a two-stage RHO methodology that exploits the modular nature of the upstream SOFC stacks by turning some of them on or off safely, infrequently, and in incremental

amounts. This leads to a modular step increase or decrease in the steady-state output of the plant, and thus the baseload can be optimally selected in order to track seasonal changes in demand as closely as possible. This allows for the CAES storage volume to be much more efficiently utilized, and significantly improves season-to-season and overall annual load-following performance. To demonstrate, this concept is applied to a SOFC/CAES plant with zero direct $CO_2$ emissions using gasified coal as a fuel source, showing for the first time that it is possible to use coal for clean, reliable and efficient electrical peaking power at the 100 megawatt scale over the entire year.

# 2. The Process and Simulation Models

## *1.1 SOFC/CAES Plant Layout*

The integrated SOFC/CAES system used for this work is shown in Figure 1, which was studied in a prior work using the "greedy" operational strategy [11] but has not been examined using a RHO framework. This system is capable of providing reliable power with system-limited peaking capabilities and 100% capture of direct $CO_2$ emissions. The essential operating principle of this plant is as follows: The plant is designed for an annual average expected power demand subject to diurnal fluctuations. During periods of low demand, the CAES system consumes electricity provided by the base-load SOFC portion to charge the CAES storage of a completely independent (save for heat integration) CAES plant. The air source for the CAES, instead of atmospheric air, is the already-compressed cathode exhaust stream (mostly $N_2$) from the SOFC power island, resulting in significant savings and efficiency losses during the compression step. The consumption of power by the CAES compressors results in a net plant output lower than the base load output of the plant, and the diverted cathode exhaust into the CAES storage may be adaptively selected in order to result in a net plant output equal to (or very close to) the demand at any given time. When demand increases beyond the base load capacity, the CAES system is discharged, pre-heated by exchanging heat with the hot SOFC exhaust streams, and expanded to generate supplemental power in order to reach the required demand.

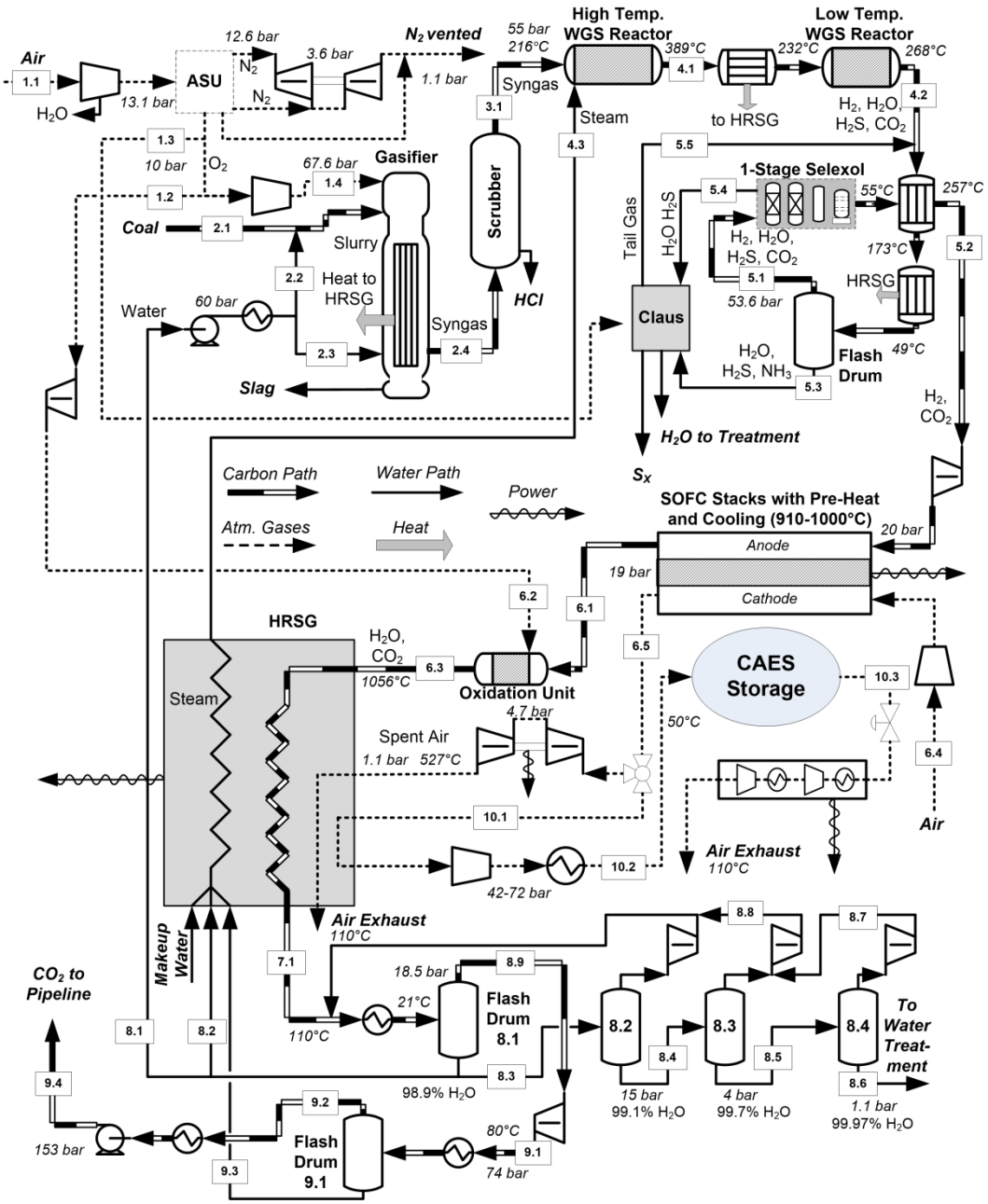


**Figure 1: SOFC/CAES plant fueled by gasified coal that is simulated with the two stage RHO scheme presented in this work. Reproduced with permission from [11]**

By synergistically using the excess heat available from the SOFC stacks (preventing the consumption of NG for pre-heating) and compressing the cathode exhaust instead of atmospheric air (reducing the overall compression ratio from 40-70 to approximately 4-7 depending on the operating pressure of the storage volume), SOFCs and CAES can be shown to complement each other nicely and result in peaking systems with higher efficiencies than any current alternative. For further details regarding the plant design and analyses, the reader is encouraged to refer to the prior studies on the design of the system [11],[22]. Please note that although this design was chosen for the case study, many other design variations, including variations using other fuels such as natural gas, are also possible.

Once constructed, some operating parameters of the SOFC/CAES plant can be changed during operation. The two key operating parameters which are changed hourly during transient operation are (1) the percentage of the cathode exhaust sent to either CAES or the heat recovery and steam generation (HRSG) section, which is controlled by the three-way valve immediately downstream of stream 6.5, and (2) the amount of compressed air released from the CAES which is controlled by the valve immediately downstream of stream 10.3. The number of SOFC stacks in operation (or equivalently, the total power output of the SOFC stacks themselves) can also be changed as a third operating variable, although only once per week.

### *2.1. Rigorous SOFC/CAES Model in Aspen Plus*

Since the rigorous SOFC/CAES system model used in this work was the same as in the prior work and is described in detail there, [11] only a brief summary is provided for brevity. Rigorous simulations of the SOFC portion of the proposed plant were performed using Aspen Plus v8.6 using the Peng Robinson equation of state (EOS) employing the Boston-Mathias modification, with a few exceptions (the Redlich-Kwong-Soave EOS and Electrolyte-NRTL packages were used for $CO_2$/$H_2O$ streams below and near the critical point of $CO_2$, respectively). The coal feedstock to the gasification step is assumed to be Illinois #6 Bituminous, and thus has a higher heating value (HHV) of 27.267 MJ/kg [23] and contains 63.75% C, 4.5% H, 1.25% N, 0.29% Cl, 2.51% S, 11.12% $H_2O$ and the remainder ash by weight [22]. The plant uses an optional water-gas shift (WGS) step upstream of the SOFC stacks to upgrade the $H_2$ content of the anode fuel stream, the trade-offs of which were addressed in the prior work. The SOFC plant is sized to produce a maximum output of approximately 820 MW, which was chosen to be consistent with our prior work and is also the size of a typical SCPC or other comparable coal-fueled base-load plant according to Woods et al. [24].

Although this is a much larger SOFC plant than any currently existing example, the US Department of Energy is anticipating that MW-scale SOFCs will exist by 2020 and should be commercially available by approximately 2030 [25],[26],[27]. In fact, Bloom Energy already has 210 kW modules available, further showing the advancement in technology is proceeding as anticipated [28]. Large-scale simulations of SOFC plants are also common in current literature [29]. It should be noted that the units in the SOFC plant are assumed to reach equilibrium, and thus the throughput of the plant may be reduced to as low as 600 MW in response to seasonal changes in base load due to the modular nature of the SOFCs. A detailed description of the SOFC plant was the topic of a prior paper and is thus not repeated here for the sake of brevity. For design decisions and stream conditions for the SOFC plant, the reader is referred to a prior work [22].

The CAES operating parameters were chosen based on the design recommendations by Luyben [30], and are comparable to the E.N. Kraftwerke plant as simulated by Raju and Khaitan [31]. Details regarding the operation and integration of the CAES system with the SOFC plant was the main topic of a prior work, and is thus not repeated here. The reader is referred to Table 1 in [11] for the assumptions related to the CAES system. The base case size of the underground CAES cavern is assumed to be 600,000 $m^3$, which was chosen based on a Pareto-optimal trade-off in the original investigation. However, with the proposed RHO framework allowing for better utilization of CAES storage volume, the size of the CAES cavern is varied in a sensitivity analysis (See section 4.2).

### *2.2. Reduced-Order SOFC/CAES Model*

The Aspen Plus simulation takes approximately 5 minutes to converge, since the model itself requires several different iterative solves to converge tear streams, design specifications, and local optimization problems. This makes it unsuitable to use in a RHO framework because the RHO algorithm, which is described in Section 3, requires around 500 simulations for the algorithm to complete (or about 40 CPU-hours) *every timestep*, which in this work is once every hour of the year. So for the entire year of interest, this would require about 40 CPU-years to compute. Furthermore, the nature of the RHO algorithm is such that it cannot be easily parallelized, so using more CPUs in parallel does not solve this problem.

Therefore, a much faster reduced-order model representing the SOFC/CAES plant was identified from the rigorous Aspen Plus model. The reduced-order model was fit by running the Aspen Plus simulation at a variety of values for three key independent state variables. These are the pressure in the CAES cavern ($P$) at the beginning of the time step, a variable related to the amount of cathode exhaust diverted to the CAES storage volume ($S$), and the current baseload capacity of the steady-state plant ($BL$). Latin hypercube sampling was used for each independent variable. For each combination of variables, the net power output of the SOFC/CAES system $f(P,S,BL)$ was computed with the Aspen Plus model and recorded. This was performed twice, such that two models were identified, one for the charging mode and another for the discharging mode. A least-squares regression method was used to identify the coefficients of the model, which had the form:

$$f(P,S,BL) = \sum_{x=0}^{2}\sum_{y=0}^{2}\sum_{z=0}^{2} a_{xyz}\left(\frac{P}{\bar{P}}\right)^{x}\left(\frac{S}{\bar{S}}\right)^{y}\left(\frac{BL}{\overline{BL}}\right)^{z}. \quad (1)$$

Note that the indexed form of this model used in the optimization routine is discussed in section 3.1.1. In the model in Eq. (1), $a_{xyz}$ is the model coefficient for the $x^{th}$, $y^{th}$ and $z^{th}$ powers of the normalized independent variables. The list of identified model parameters is shown in Table 1. The overbar denotes the value at which each of the variables were normalized to improve the scaling accuracy of the model. It is convenient to note the relationship between the variable used to describe the exhaust flow rate $(S)$, the flow rate of the cathode exhaust $(F)$, and $BL$ is:

$$S = \begin{cases} 1 - \frac{F}{50.257BL - 3123.4} & [when\ charging\ CAES] \\ F & [when\ discharging\ CAES] \end{cases} \quad (2)$$

A plot showing the nonlinear fit of the model and sampled data points for a variety of baseloads (each represented by a different plane) are shown in Figure 2. It can be seen that the model fits the data very well without spurious curvature or significant biases, with an overall testing $R^2$ value of 0.989 and a root-mean squared error of estimation (RMSEE) of 2 MW (0.4%). A testing set, also sampled using Latin Hypercubes, was used to validate the model, which had a similar $R^2$ and a root-mean squared error of prediction (RMSEP) of 5 MW (1.0%). Figure 3 shows the comparative results of the reduced-order model versus the output of the full model for a variety of pressures, flows, and baseload values (all independent variables in the model). It can be seen that the data are very tightly correlated (corresponding to the strong goodness of fit) and are well scattered around the $y = x$ line for all SOFC/CAES plant outputs, showing that the model is not over-fit, nor is the shape of the model biased in any regions of the typical operating regime. Higher order polynomial terms did not increase the $R^2$ significantly and had small coefficient values, and so only 2nd order terms were used in the final reduced model.

**Table 1: Reduced-order model coefficients for revised RHO formulation**

| Coefficient | **Value** when $\boldsymbol{m = c}$ **(charging mode)** | Value when $\boldsymbol{m = d}$ **(discharge mode)** |
|---|---|---|
| $\mathbf{a_{000}}$ | 173.3 | 0.1 |
| $\mathbf{a_{100}}$ | -158.0 | 0 |
| $\mathbf{a_{200}}$ | 24.6 | 0 |
| $\mathbf{a_{010}}$ | -55.8 | 25.5 |
| $\mathbf{a_{020}}$ | 6.2 | 0 |
| $\mathbf{a_{001}}$ | 369.4 | 696.8 |
| $\mathbf{a_{002}}$ | 79.6 | 0 |
| $\mathbf{a_{011}}$ | 94.5 | 0 |
| $\mathbf{a_{101}}$ | 12.7 | 0 |
| $\mathbf{a_{110}}$ | 70.7 | 0 |
| $\mathbf{a_{111}}$ | -25.4 | 0 |

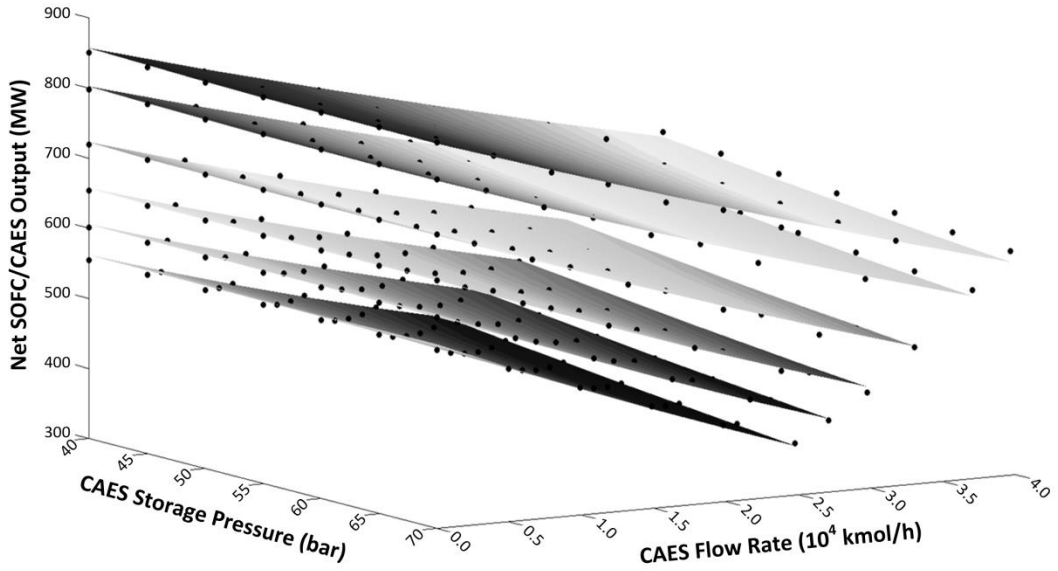


**Figure 2: Predicted (planes) and simulated (dots) performance of the reduced-order SOFC/CAES model used in this work for six selected baseline capacities (BL).**

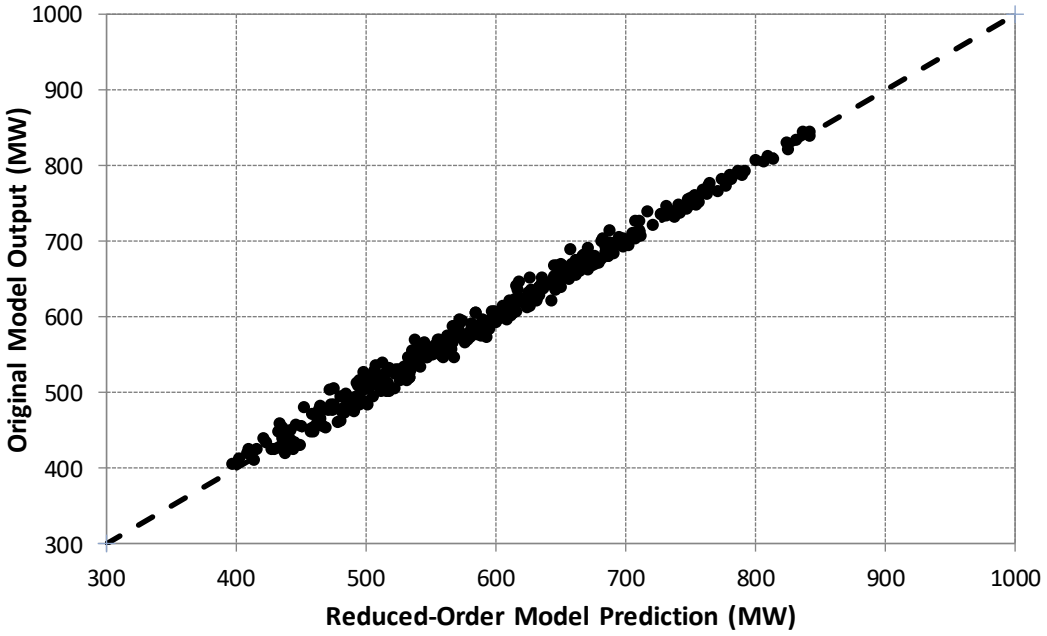


**Figure 3: Correlation plot comparing the output of the reduced order model described in section 2 (x-axis) to the detailed Aspen Plus model of the SOFC/CAES plant (y-axis) for a range of operating conditions using Latin Hypercube sampling**

# 3. Two-Stage Rolling Horizon Optimization Framework

The reduced-order model was implemented in GAMS [32]. The RHO algorithm was implemented in MATLAB, which communicated with GAMS to perform the optimization routine at each simulated time step. The RHO problem formulation for both stages and a discussion of what solvers were used in GAMS is presented in this section.

## *3.1. Problem Formulation*

In the load-following optimization case, it is the objective of the RHO to determine the SOFC/CAES operating parameters over the control horizon that will either minimize the sum-of-squared errors (SSE), maximize the total revenue, or some weighted combination of both over the optimization's horizon ($\mathcal{R}$). The primary decision variables of interest determined by the RHO program are the flow rate to or from the CAES cavern ($F$) and what the baseload for the coming week should be ($BL$), which is then used to calculate the power output of the combined SOFC/CAES plant at each time step.

### 3.1.1. First Stage Objective Function Formulation

The problem formulation for this investigation is inspired by the formulation in our prior work [21] with some significant changes to the formulation and solution strategy for improved load-following and revenue generation performance. Overall, the RHO objective attempts to maximize a weighted objective function $\Phi$ that balances the total revenue generated by the SOFC/CAES plant ($\mathcal{R}$) and the load following performance of the plant as measured by the negative of the sum of squared error (SSE) between the plant output and demand as follows:

$$\max_{\delta_{i,t},\, F_{i,t}} \Phi_i = \{\psi \mathcal{R}_i - (1-\psi) SSE_i\}, \tag{3}$$

$$SSE_i = \sum_{t=1}^{N} \left(E_{i,t} - D_{i,t}\right)^2, \tag{4}$$

$$\mathcal{R}_i = \sum_{t=1}^{N} \left(E_{i,t}\omega_{i,t}\right), \tag{5}$$

where $SSE_i$ is the sum of squared error difference at each simulation time step $i$ between the power produced $E_{i,t}$ and forecasted demand $D_{i,t}$ (both in MW) at each control move $t$ across the forecast time horizon $N$, $\omega_{i,t}$ is the forecasted market spot-price of electricity (POE) for each one-hour optimization interval over the optimization horizon (both forecasts are obtained from the IESO [33]), and $\psi \in [0,1]$ defines the emphasis on which of the two objectives should be met. Selecting $\psi = 1$ results in a pure revenue maximization problem while selecting $\psi = 0$ yields a load-following problem. $F_{i,t}$ is the flow rate to or from the CAES storage volume at each simulation time step, the direction of which is denoted by $\delta_{i,t}$, which is a binary variable that denotes whether the CAES storage is being charged ($\delta = 1$; the net plant output is reduced below the base-load) or discharged ($\delta = 0$; the net plant output is increased beyond the base-load). For the demonstrative purposes of this work, $i$ ranges from 1 to 8760, for each of the 8760 hours in one simulated year of plant operation. However, it is possible for this routine to be used indefinitely in real time, thereby not having a terminal value of $\xi$.

### 3.1.2. Process Model Equations

For the purposes of this investigation, the optimization or "control move" interval is one hour. $E_{i,1}$ is therefore the power actually produced at simulated timestep $i$, and $E_{i,t}$ is the power the optimizer plans on producing $t$–1 timesteps in the future for $t = (2 \dots N)$, which may or may not be implemented depending on future decisions since the entire forecasted output is recalculated at each update of $i$. The optimal production of the plant at the current simulation time $i$ for the prediction horizon $t = 1 \dots N$ is calculated as:

$$E_{i,t} = \delta_{i,t} f_{c,i,t}\left(P_{i,t}, S_{i,t}, BL_i\right) + \left(1 - \delta_{i,t}\right) f_{d,i,t}\left(P_{i,t}, S_{i,t}, BL_i\right), \tag{6}$$

where $BL_i$ is the baseload selected for the current simulation timestep $i$ (the optimization sub-routine to select $BL_i$ is discussed later), $E_{i,t}$ is the electrical output of the SOFC/CAES plant for RHO horizon $t = 1 \dots N$ at simulation time step $i$, $D_{i,t}$ is the demand for the RHO horizon $t = 1 \dots N$ at simulation time step $i$. The variables $S_{i,t}$ and $P_{i,t}$ are the variable related to the molar flow rate to/from the storage cavern (in kmol/hr) and the pressure (in bar) in the cavern at each time step, respectively, and $f_{m,i,t}$ are the indexed versions of the reduced-order models for the charging and discharging of the CAES cavern where $m \in \{c, d\}$, respectively and take the form:

$$f_{m,i,t}\left(P_{i,t}, S_{i,t}, BL_i\right) = \sum_{x=0}^{2}\sum_{y=0}^{2}\sum_{z=0}^{2} a_{xyz} \left(\frac{P_{i,t}}{\bar{P}}\right)^x \left(\frac{S_{i,t}}{\bar{S}}\right)^y \left(\frac{BL_i}{\overline{BL}}\right)^z, \tag{7}$$

$$S_{i,t} = \begin{cases} 1 - \frac{F_{i,t}}{50.257 BL_i - 3123.4} & when\ m = c \\ F_{i,t} & when\ m = d \end{cases}. \tag{8}$$

Note that the description of the coefficients is given in the previous section and the values of which are listed in Table 1. The mass balance constraint on the CAES cavern is described by:

$$n_{i,1} = n_{i-1,1} + F_{i,1}\delta_{i,1}\Delta - F_{i,1}(1-\delta_{i,1})\Delta,$$
$$n_{i,t} = n_{i,t-1} + F_{i,t}\delta_{i,t}\Delta - F_{i,t}(1-\delta_{i,t})\Delta, \qquad [\forall\, t = (2 \dots N)] \tag{9}$$

where $n_{i,t}$ is the number of moles of cathode exhaust contained in the CAES storage volume at any given timestep $i$ and $\Delta$ is the length of the simulation time step in which the output of the plant is held constant via a zero-order hold. Note again that $n_{i,1}$ is the actual molar holdup of the cavern as a result of executing the decision variables $F_{i,1}$ and $\delta_{i,1}$, and $n_{i,t}$ for $t = (2 \dots N)$ is the predicted molar holdup $N-1$ timesteps in the future based on the current optimization results, and may or may not change in the future. The pressure $P_{i,t}$ of the CAES storage volume is calculated using the SRK equation of state:

$$P_{i,t} = \frac{RT_{i,t}}{\mathcal{V}_{i,t} - b_{SRK}} - \frac{a_{SRK}}{T^{0.5}\mathcal{V}_{i.t}(\mathcal{V}+b_{SRK})}, \qquad [\forall\, t = (1 \dots N)] \tag{10}$$

where $a_{SRK}$ and $b_{SRK}$ are the SRK model coefficients for the cathode exhaust (assumed to be pure $N_2$) with values of $1.56 \times 10^{-5}\ \frac{m^6\, bar}{mol^2}$ and $2.67 \times 10^{-5}\ \frac{m^3}{mol}$, respectively [34]. The symbol $R$ is the universal gas constant and $T$ is the uniform temperature in the storage volume (assuming the contents of the volume itself are well-mixed). The molar volume of the CAES cavern contents at each control step is denoted by $\mathcal{V}_{i,t}$ and is determined as a function of the CAES storage volume $V$ as:

$$\mathcal{V}_{i,t} n_{i,t} = V. \qquad [\forall\, t = (1 \dots N)] \tag{11}$$

Note that the molar volume calculations given above in Eq. (11) combined with the material balances in Eq. (9) result in nonlinear relationships between the pressure in the CAES cavern and the flow rate to or from its control volume, which increases the complexity of the constraint in Eq. (10). Pressure is calculated at each time step to ensure that it never exceeds the operating limits of the CAES system, specifically:

$$P_{min} \le P_{i,t} \le P_{max}. \qquad [\forall\, t = (1 \dots N)] \tag{12}$$

Finally, the flow rate into the CAES cavern is bounded by the cathode exhaust flow rate denoted by $F_{max}$:

$$0 \le \delta_{i,t} F_{i,t} \le F_{max}. \qquad [\forall\, t = (1 \dots N)] \tag{13}$$

Inspection of the above equations shows that $E_{i,t}$ is a quadratic function in $P_{i,t}$, $BL_{i,t}$ and $S_{i,t}$. However, $P_{i,t}$ is itself a highly nonlinear function of $F_{i,t}$ and thus $S_{i,t}$ due to the SRK equations of state and material balances on the CAES storage volume. It can therefore be concluded that the objective function for this problem is highly nonlinear and includes the binary variable $\delta_{i,t}$ at each simulation timestep. The RHO problem at each simulation timestep $i$ is thus a mixed-integer nonlinear program (MINLP), the size of which increases depending on the forecasting and optimization horizon $N$.

### *3.2. Second Stage: Baseload Selection*

The baseload $BL_i$ is adjusted every $\xi$ time steps of the simulation (chosen to be one week, or 168 hours, due to the desired low-frequency of changing the SOFC output) by solving the second stage optimization problem of the form:

$$\min_{BL_i} \Gamma = \left\{ \min_{\delta_{\iota,\tau} F_{\iota,\tau}} \left[ \sum_{\iota=i}^{i+\xi} \sum_{\tau=1}^{N=1} \left( E_{\iota,\tau} - D_{\iota,\tau} \right)^2 \right] \right\}, \tag{14}$$

$$BL_\iota = BL_i, \qquad [\forall\, \iota] \tag{15}$$

$$(BL_i - BL_{i-1})^2 \leq (\Delta BL_{max})^2, \tag{16}$$

where $\Delta BL_{max}$ is the maximum permitted change in the baseload (40 MW was used in this work) every $\xi$ timesteps. It can immediately be seen that the objective function in Eq. (14) is the minimization of the original RHO objective function focused entirely on the minimization of SSE as described in equations (1) and (2). However, the RHO horizon for the sub-problem is restricted to one future time step ($N = 1$), a technique known as the greedy algorithm. The optimization problem in Eq. (14) is subjected to the same operating constraints as the original RHO problem, but in this case $BL_i$ is adjusted to find the baseload that minimizes the SSE of the greedy algorithm for the coming week. The outer optimization problem is thus restricted to a nonlinear program of one dimension that can be solved much more quickly than the full-sized inner optimization problem outlined in Eq. (3). The only additional constraint for Eq. (14) is the restriction that $BL_i$ must not move more than $\Delta BL_{max}$ from the previous value (Eq. 16).

As a final note, it should be stated that the final result of the outer-layer optimization problem in Eq. (14) is rounded to the nearest MW step change to represent the modular nature of the SOFC stacks and thus the gross output of the SOFC/CAES plant. Rounding to the nearest 5 MW has been found to not change the nature of the solution to the outer-layer RHO problem, and thus is not added as a hard constraint to avoid having $BL_i$ appear as an integer variable

### *3.3. Optimization Scheme and Method*

#### 3.3.1. Summary of Optimization Algorithm

The optimization scheme in this work follows closely to that of the prior investigation [21]. However, in this case there is an additional outer-layer optimization that occurs every $\xi$ time steps. A summary of the algorithm is as follows:

1. Select desired values of the objective weighting factor $\psi$, the storage cavern volume $V$, and the RHO horizon $N$.

2. Initialize the problem with the demand predictions for next $N$ timesteps (The actual historical hourly operation of 2014 is used for this study).

3. Provide the initial guesses for the SOFC/CAES plant output ($\dot{E}$), number of moles in the cavern ($\dot{n}$), model selection variable ($\dot{\delta}$) and operating pressure of the cavern ($\dot{P}$) to improve the likelihood of locating an optimal solution:

**If** $i = 1$

$\dot{E}_{1,1} \dots \dot{E}_{1,N} = D_1 \dots D_N$

$\dot{n}_{1,1} \dots \dot{n}_{1,N} = n_0$

$\dot{\delta}_{1,1} \dots \dot{\delta}_{1,N} = 1$

$\dot{P}_{1,1} \dots \dot{P}_{1,N} = P_0$

**Else**

$\dot{E}_{i+1,1} \dots \dot{E}_{i+1,N-1} = E_{i,2} \dots E_{i,N}$ $\quad$ $\dot{E}_{i+1,N} = D_{i+N}$

$\dot{n}_{i+1,1} \dots \dot{n}_{i+1,N-1} = n_{i,2} \dots n_{i,N}$ $\quad$ $\dot{n}_{i+1,N} = n_{i,N}$

$\dot{\delta}_{i+1,1} \dots \dot{\delta}_{i+1,N-1} = \delta_{i,2} \dots \delta_{i,N}$ $\quad$ $\dot{\delta}_{i+1,N} = \delta_{i,N}$

$\dot{P}_{i+1,1} \dots \dot{P}_{i+1,N-1} = P_{i,2} \dots P_{i,N}$ $\quad$ $\dot{P}_{i+1,N} = P_{i,N}$

4. Assign the appropriate baseload:

**If** $i = 1$ **OR** $\xi \ (mod\ t) = 0$:

Perform **second stage RHO** to select optimal baseload $BL_i$

**Else**

$BL_i = BL_{i-1}$

5. Pass in demand, the current baseload, and the operating conditions of the CAES system to the **first stage RHO** and obtain results.

6. Recover the actual values at simulation step $i$ for plant output ($\bar{E}_i$), cavern pressure ($\bar{P}_i$) and number of moles ($\bar{n}_i$) as the first value of each described by the rolling horizon optimizer.

$\bar{E}_i = E_{i,1}$

$\bar{P}_i = P_{i,1}$

$\bar{n}_i = n_{i,1}$

7. Update simulation time step and save results: $i = i + 1$ . Check if $i > N_{max}$, which denotes the end of the simulation:

**If** $i > N_{max}$

End the algorithm.

**Else**

Return to step 3.

It is important to note that for research purposes, the demand for the entire year was "known" up front so that each iteration of the algorithm could take place immediately. However, in a real

application, demand forecasts for the next $N$ timesteps would be used instead, and one iteration would take place each hour over the course of the year. Also, in the case of the Ontario grid, the existing 24-hour demand forecast prediction models are very good with a low prediction error (typically less than 4%) [33]. Our prior work for the one-layer RHO [21] showed that the difference in performance between using predictions with up to 12% error versus perfectly accurate predictions was small due to the structure of the RHO framework. Therefore, only perfectly accurate predictions are used in this study to determine a "best case" scenario.

### *3.4. Solver Selection*

Two commercial solvers were used in GAMS in a hierarchical structure for this work: ANTIGONE and BARON [32]. ANTIGONE is used as the primary solver in this case because it was found to solve each optimization step of the simulation faster than BARON when provided with a feasible initial guess (solution time for $N = 24$ is approximately 20 seconds with ANTIGONE). However, if a feasible initial guess was not provided by the algorithm presented in section 3.3.1 due to a switch in $\delta$ or an unexpectedly large change in demand or price, ANTIGONE sometimes failed to converge to a feasible solution. In these cases, it was found that BARON was able to solve the problem to a feasible optimum (solution time for $N = 24$ is approximately 10 minutes) in all cases. Consequently, a feasible optimum was found at each simulation time step, which was recorded in MATLAB. The total time for one simulation of 8760 time steps (one year of operation with hour-long control intervals) was approximately 5 CPU days per run, on average. Note that if BARON were used exclusively, approximately 61 CPU days would have been required.

## 4. Results and Discussion

The following sections describe the impacts that the proposed two-stage RHO scheme has on the load-following and revenue-maximization capabilities of the studied SOFC/CAES plant fueled by gasified coal. All simulation case studies use a forecasting and optimization horizon of $N = 24$ hours (one full day ahead) and $\xi = 168$ hours (one full week ahead). It should be noted that the effect of adjusting the horizon of $N = 24$ hours to be the set $N = \{6, 12, 24, 48, 168\}$ was discussed in our prior work that focused on the design and application of a single-stage RHO methodology [21]. Since the value of $N$ only affects the performance of the first stage of the proposed two-stage RHO strategy, it is very likely that the week-to-week results for the two-stage using different values of $N$ will be similar to the prior work.

### *4.1. Effect of Two-Stage RHO Scheme on Plant Performance*

The importance of being able to change the baseload output of the integrated SOFC/CAES plant is demonstrated in Figure 4, which shows the average weekly demand for the province of Ontario, Canada for the operating year of 2014 scaled to an average of 720 MW. Since the CAES system storage capacity is on the order of 100s of MW-h, it would be impossible to exclusively use CAES to account for seasonal drifts in demand such as those shown in Figure 4 without an intractably large storage volume. Furthermore, the maximum range of the power change achievable by the CAES system is constrained by the cathode exhaust flow rate (when charging, or dipping below the current baseload) and excess heat available from the SOFC for pre-heating (for discharging, or rising above the current baseload). This range, for a 720 MW baseload plant,

is approximately 200 MW if the baseload is never changed. However, it can be seen in Figure 4 that the difference between the minimum and maximum average weekly demand is nearly 235 MW, with the actual difference between the highest and lowest moments of the year being 527 MW. Thus, the use of weekly optimal baseload changes allows for more efficient use of the CAES storage volume and operating constraints.

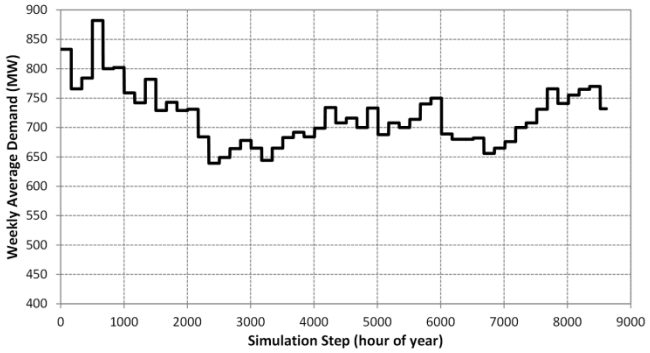


**Figure 4: Weekly average demand for the simulated market over one year of operation**

### 4.1.1. Load Following Performance

Shown in Figure 5 is the simulation results for one consistently high week of demand near the beginning of the year. Figure 5 (B) shows the performance of the SOFC/CAES system with the default selected initial value for *BL* of 720 MW (recall that this is the average demand over the entire simulated year) while Figure 5(A) shows the performance of the same system with an optimally selected *BL* of 830 MW (note that all subsequent changes to BL after this initial selection are subjected to the constraint of Eq. 15). It can readily be seen that the load-following capabilities of the integrated SOFC/CAES system are far greater when the baseload is chosen optimally, with over a 99% improvement in the load-following metric as measured by SSE. It is still clear in Figure 5(B) that the first-stage RHO scheme is attempting to use the forecasted demand to reduce large misses, but due to the low baseload output of the plant, the CAES storage volume cannot be utilized effectively. This result is demonstrated in Figure 6(B), which shows the operating pressure of the CAES storage volume for the same week of operation. It is clear that the entire energy storage capacity of the CAES system is underutilized, primarily due to demand being consistently higher than the base load can even achieve (and thus no excess energy is available for storage). Compare this result to Figure 6(A), which shows that the entire storage capacity of the CAES storage volume is utilized (both the maximum and minimum operating pressures are reached). Furthermore, it can be seen that the operating limits are touched upon but are not active for significant periods of time. This is due to the combined optimal selection of the baseload output of the plant via the second layer of the RHO scheme and the optimal hourly output as chosen by the first layer.

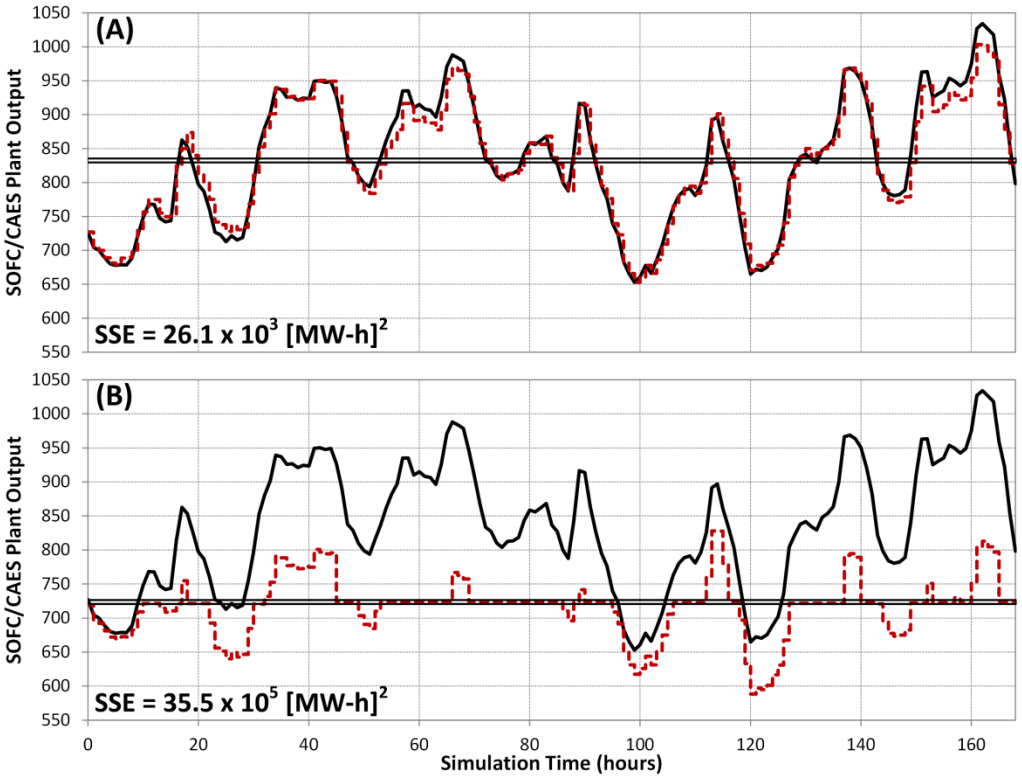


**Figure 5: SOFC/CAES plant simulation results (red dashed line) and market demand (black line) for a high-demand week of operation near the beginning of the year. (A): with optimal base load selection using both layers of the RHO scheme. (B): With default base load selection using only the first layer of the RHO scheme**

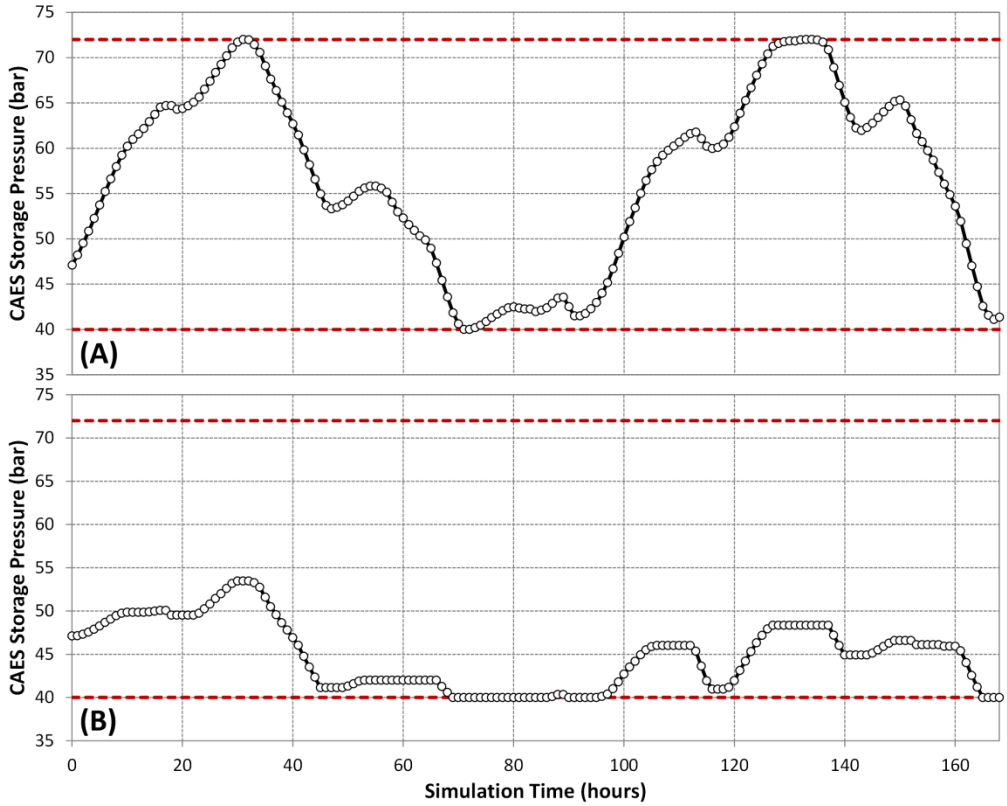


**Figure 6: CAES storage volume pressure profiles for the high-demand simulated week of operation. (A): with optimal base load selection using both layers of the RHO scheme. (B): With default base load selection using only the first layer of the RHO scheme**

Shown in Figure 7 is another case week that demonstrates the improvements brought about by the augmentation of the RHO scheme presented in this work, but for a week of consistently low-demand. In Figure 7(A), it is clear that the optimally selected baseload of 645 MW allows for more efficient use of the CAES storage, resulting in a load-following improvement of approximately 95% as measured by SSE for this week. It is clear in Figure 7(B) that the one-layer RHO scheme is optimizing the hourly output of the plant based on the constraints imposed by the CAES storage volume limits (and thus avoiding big misses by having a more consistent demand/supply mismatch), but in general the ability to provide the precise demanded power is nearly impossible. This is emphasized in Figure 8, which shows the pressure profiles for the CAES storage volume with (Figure 8[A]) and without (Figure 8[B]) the second layer of the RHO scheme choosing the optimal baseload for the week ahead. However, Figure 8(B) is in contrast to Figure 6(B) since in this case the CAES storage volume is always operating at or near its maximum limit due to the non-optimized baseload plant being too large and thus wasting power (and the resources used to make it). Compare this with Figure 8(A), which clearly shows that the entire operating range of the CAES storage is used, leading to a more efficient utilization of the available storage. In addition, it is also clear that simply oversizing the baseload and leaving it at that same level all year round as a strategy for ensuring that high-demand weeks are met is grossly inefficient and was the original motivation for the design of the integrated SOFC/CAES plant [11]. Note that the difference in initial pressures for each panel in Figure 8 are due to different operation decisions made prior to the highlighted week of operation.

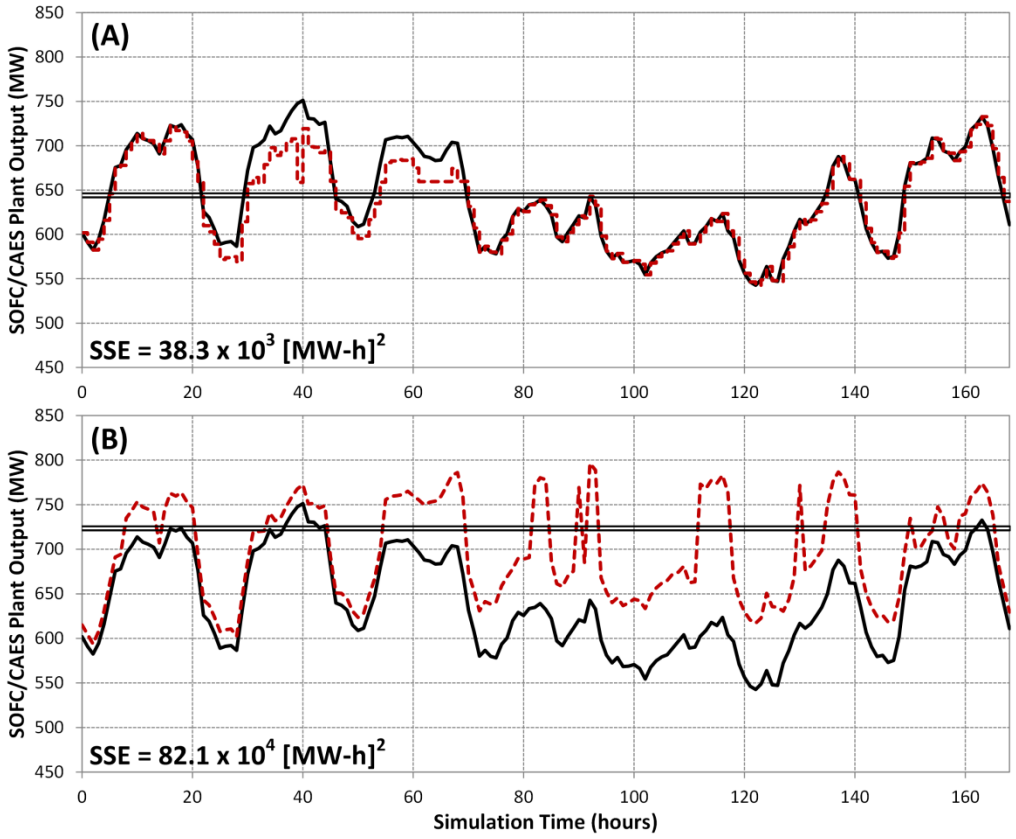


**Figure 7: SOFC/CAES plant simulation results (red dashed line) and market demand (black line) for a low-demand week of operation near the beginning of the year. (A): with optimal base load selection using both layers of the RHO scheme. (B): With default base load selection using only the first layer of the RHO scheme**

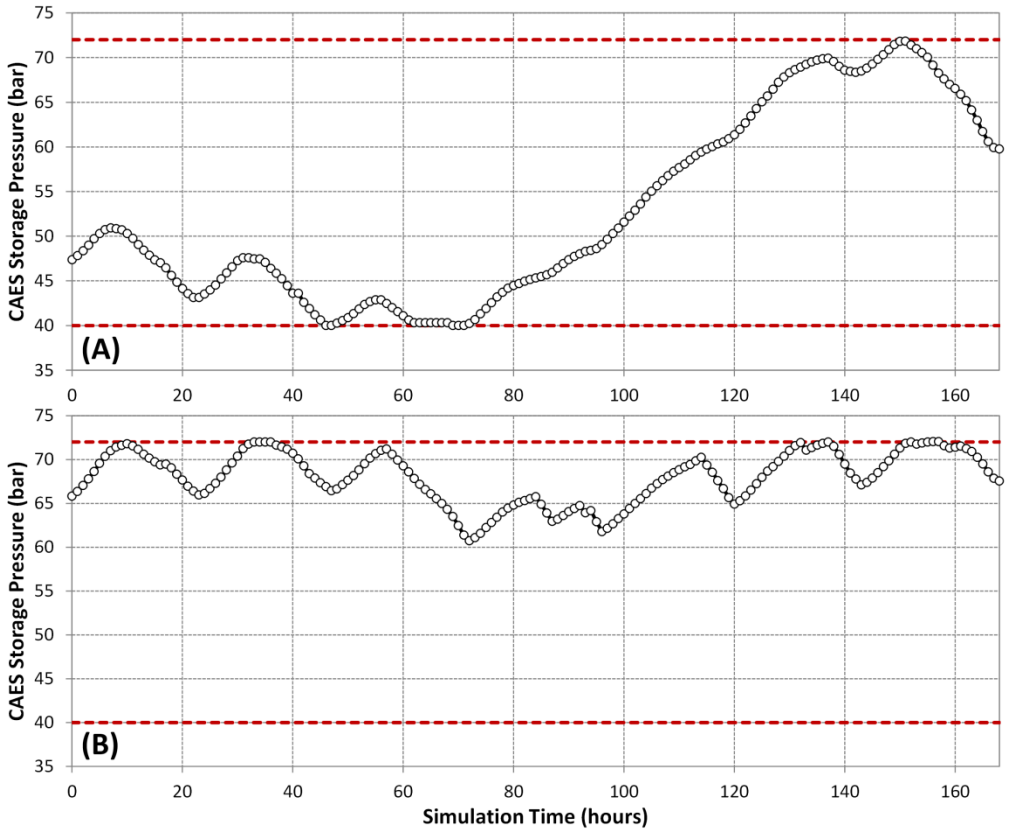


**Figure 8: CAES storage volume pressure profiles for a low-demand simulated week of operation. (A): with optimal base load selection using both layers of the RHO scheme. (B): With default base load selection using only the first layer of the RHO scheme**

In the previous work, the one-layer RHO scheme provided a significant load-following improvement for certain weeks of operation, but only those consistently at or near the default baseload output of 720 MW. The adaptive selection of the baseload output of the plant offered by the new second layer of the proposed RHO method allows for effective utilization of the CAES storage volume during any week of the year. This is further reinforced by the fact that the second layer takes the available CAES storage into account when selecting the baseload for the coming week. The importance of selecting the baseload each week is exemplified in Figure 9, in which it can be seen that the baseload is adjusted nearly every week to adapt to seasonal drifts in demand.

With regards to the annual load-following performance of the integrated plant, a figure is not shown since the high number of data points would make the plot virtually illegible. Rather, the SSE values for a one-year simulation are provided in Table 2. It is clear that, over an entire year of operation (8760 first-layer optimizations with $N = 24$ and 52 second-layer optimizations with $\xi = 168$) the proposed two-level RHO scheme can meet demand with a total SSE of $4.15 \times 10^6$ (MW-h)$^2$. This may be compared to the use of the single layer RHO developed in the prior work for the same year of demand using a fixed baseload of 720 MW, which is an order of magnitude higher at $30.3 \times 10^6$ (MW-h)$^2$. Furthermore, employing the greedy algorithm (hourly decisions with no forecasted optimization, equivalent to the one-layer scheme with $N = 1$) with a fixed baseload for this year of demand results in an SSE of $42.7 \times 10^6$ (MW-h)$^2$. The proposed two-level RHO method designed to exploit the modular nature of the SOFC stacks can thus improve the load-following performance of an integrated SOFC/CAES peaking plant by over 90% when

compared to using no optimization at all, and 86% when compared to optimizing the hourly operation of the CAES system exclusively. Although it is not possible to achieve perfect load-following from a stand-alone SOFC/CAES plant due to the operating limits and constraints of the CAES system, more efficient utilization of the CAES storage volume by appropriately optimizing the weekly baseload is possible; it is therefore likely that increasing the CAES storage volume beyond the base-case 600,000 $m^3$ will result in even better load-following, but with diminishing returns. The effect of CAES storage on annual load-following capabilities is discussed later in section 4.2.

Another metric in Table 2 that shows the improvements brought on by the two-level RHO is the number of times the CAES storage pressure is near its upper or lower bound. Over the year, the two-level RHO scheme results in the CAES storage pressure dipping below 41 bar (that is, the CAES storage is near or at the minimum allowable pressure) 423 times (4.8% of the total time steps). Of those 423 occurrences, the CAES pressure was stuck at the lower bound for more than one time step in a row at only 83 of them (0.9% of all time steps). Compare this to the one-layer RHO scheme for the same simulation, in which the CAES storage pressure was at or near its minimum constraint 990 times (11.3%). Of those 990 instances, 384 of them (4.4%) occurred consecutively. This indicates that nearly 4.5% of all demand instances, even with the one-layer RHO active, resulted in consecutive time steps in which the CAES system went unused due to capacity constraints. By reducing this occurrence to less than 1% of all time steps simulated, it is clear that the two-level RHO is much more effective at utilizing the limited CAES storage volume when demand is consistently lower than the average value of 720 MW. A similar result occurs with regards to the CAES storage volume operating at or near its maximum allowable pressure. Throughout the year, the two-level RHO results in the CAES storage pressure rising above 71 bar (within 1 bar of maximum) 288 times (3.3% of the year), whereas the one-layer RHO allows this to happen 622 times (7.1% of the year). Of the 288 instances where the two-level RHO results in operation near the maximum pressure constraint, only 38 of them (0.4%) result in consecutive time steps at maximum pressure, compared to 96 (1.1%) for the one-layer RHO.

Moreover, the two-level RHO results in the maximum and minimum pressures of the CAES storage volume being reached during the *same week* on 21 occasions versus only 5 for the one-layer RHO, indicating that the baseload is being selected so as to optimally utilize the available CAES storage. These pressure constraint results further reinforce that the two-level RHO makes much better use of the limited CAES storage capacity, which allows for much better load-following on an annual basis.

Note finally that in order for the two-level RHO scheme to be effective, a larger baseload amount of SOFC stacks would have to be purchased than the averaged-out 720 MW. The total size of the baseload SOFC power island would therefore have to be its maximum output of 830 MW, which is approximately 15% higher than the size of the plant used in the one-layer RHO. Although a full economic impact analysis is outside of the scope of this work, the increase in capital investment comes with two inherent benefits that should be considered: (1) because more of the demand is met, more power can be sold, and (2) the fuel consumption of the plant, which is the largest contributor to operating cost, is actually lower for the 830MW plant using the two-level RHO than the one-layer RHO case by a small margin (0.7%) while meeting higher peaks than possible for the one-layer method.

**Table 2: Load following metrics comparing this work to the methods used in prior studies**

| | Greedy Policy (no RHO) | One-Level RHO | Two-level RHO (This Work) |
|---|---|---|---|
| SSE ($10^6$ [MW-h]$^2$) *Lower is better* | 42.7 | 30.3 | 4.15 |
| Time steps within 1 bar of pressure bound *Lower is better* | 4715 | 1612 | 711 |
| Consecutive time steps at upper or lower bound *Lower is better* | 3781 | 480 | 121 |
| Weeks in which maximum and minimum pressure are both visited *Higher is better* | 2 | 5 | 21 |

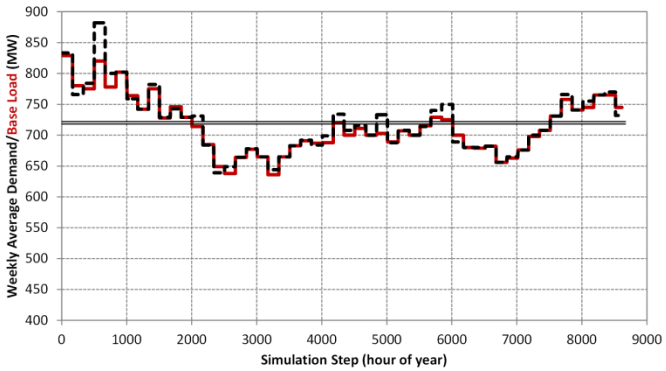


**Figure 9: Weekly average demand (black line) for the simulated market over one year of operation alongside the optimally selected weekly baseload (red line) via the second stage of the proposed RHO method. The double-line is the constant average 720 MW chosen by the one-level RHO**

### 4.1.2. Economic Performance

Shown in Table 3 are the resulting revenues generated by the SOFC/CAES plant over the simulated year of operation based on the actual market spot-price of electricity over that span. For each result, the same values of $N = 24$ and $\xi = 168$ are used as in the load-following scenario, but in this case the economic parameter $\psi$ is varied from 0 (a purely load-following objective) to 1.0 (a purely economically driven objective that foregoes matching supply and demand in an attempt to maximize revenue) for the first layer of the RHO scheme. Note that price forecasting models are generally much less reliable than demand forecasting models, and thus the use of the proposed RHO scheme is likely better suited for a load-following scenario as concluded in the prior work. Also note that the use of a revenue maximization objective in the first stage of the proposed two-level RHO scheme results in an attempt to maximize revenue while still following the seasonal trends of demand. The reason for this is simply because it is unrealistic to expect to be able to sell the maximum possible capacity of the SOFC/CAES plant to the market for the entire year, which would be the exclusive optimization decision since there is no negative cost associated with overproduction included in the given problem formulation. Consequently, the second stage of the simulation selects a baseload most appropriately suited to the coming week of demand in the same fashion as the load following objective, but the first level of the RHO is free to produce whatever results in the highest revenue generation possible. In reality, there are a multitude of potential objective function reformulations that may consider operating cost, annualized capital costs, or any combination of these that also consider operating constraints (such as minimum production constraints or constraints on maximum allowable misses). The following case study

results are meant to show that the proposed two-level RHO is adaptable and may readily be implemented with an economic objective of the user's choosing.

Results for this case study show that it is possible to use the two-level RHO to increase annual revenue by as much as $14.1 million (6.3%) over the load-following scenario by using the CAES storage to exploit future jumps or drops in the spot price of electricity. This is unsurprising, since the currently existing CAES plants use this concept as their primary motivation to employ CAES technology, as mentioned earlier. However, this increase in revenue does not come without a trade-off, as the load-following portion of the objective function is eschewed entirely, leading to a very sporadic supply profile such as that shown in Figure 10. Based on the results in Figure 10, any scenario requiring distributed power generation or other cases in which high reliability and availability is needed would not be an appropriate opportunity to use the revenue maximization method. The application of the economic objective function is rather to utilize the available CAES storage for a given week of operation based on a previously selected baseload.

Given the continuous nature of the economic weight $\psi$, it is possible to achieve a hybridized objective function that balances revenue generation and delivering reliable power. A discussion revolving around this concept and the trade-offs associated with it are provided in section 4.3.

**Table 3: SSE results comparing this work to the methods used in prior studies**

| Economic Parameter $\psi$ | **Revenue Generated ($10^6$ $)** | **Revenue Relative to Base Case** |
|---|---|---|
| **0.00** | **224.6** | **100.0%** |
| **0.50** | **229.2** | **102.0%** |
| **0.75** | **233.8** | **104.1%** |
| **0.90** | **238.4** | **105.6%** |
| **0.95** | **238.6** | **106.2%** |
| **1.00** | **238.7** | **106.3%** |

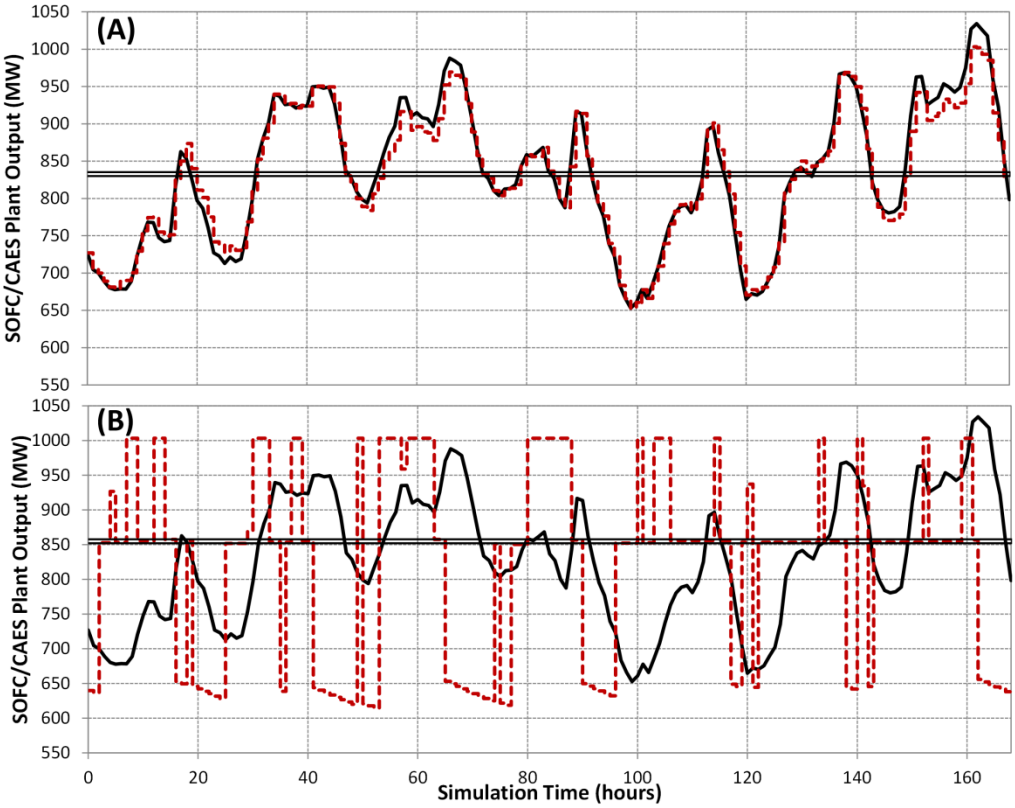


**Figure 10: SOFC/CAES plant simulation results (red dashed line) and market demand (black line) for the consistently high week of operation near the beginning of the year using the proposed two-level RHO. (A): with the economic weighting parameter $\psi = 0$. (B): with the economic weighting parameter $\psi = 1$**

## *4.2. Effect of Storage Volume on Plant Performance*

In the original work defining the conceptual plant design of an integrated SOFC/CAES system for peaking power, it was postulated that increasing the CAES volume would improve the load-following capabilities of the integrated plant [13]. Although a sensitivity analysis in that work showed that such improvements are possible, they were not without significant added cost and exhibited a significant case of diminishing marginal return for increasing the size of the CAES storage volume. This result was primarily due to the CAES system only capable of storing intermediate amounts of energy (hundreds of MW-h), but the seasonal drifts in demand required massive amounts of energy storage (nearly millions of MW-h) that were not possible with CAES unless an excessively large volume was available. Moreover, as previously mentioned, the maximum amplitude of the CAES system is not sufficient to handle the maximum and minimum swing in demand observed by a typical market.

However, the adaptive baseload selection routine introduced in this work allows for a much more efficient utilization of the CAES volume throughout seasonal drifts in demand. As a result, a sensitivity analysis was performed to assess what improvements to load following would be possible with modest increases in the base case CAES volume size. The results showing the annual SSE for the integrated SOFC/CAES plant using the proposed two-level RHO with $N = 24$, $\xi = 168$ and $\psi = 0$ versus the available CAES storage volume (with all other operational constraints the same) are shown in Figure 11. As expected, Figure 11 shows diminishing marginal returns as

a function of CAES storage volume size. However, doubling the CAES cavern to (a very reasonable) $1.2 \times 10^6$ $m^3$ results in a 53% reduction in SSE (from $4.15 \times 10^6$ to $1.95 \times 10^6$ [MW-h]$^2$) over a year of operation. Furthermore, doubling the storage size results in its operating pressure being within 1 bar of the maximum or minimum constrained range for only 339 time steps (or 3.9% of the year). This is nearly a 20% reduction compared to the base case cavern size. Along with this reduction in operation near the constraints, the number of instances where the CAES pressure constraint is nearly active for consecutive time steps is only 45 times in this scenario, further reinforcing that the larger CAES volume is being efficiently used by the RHO scheme to improve the load-following capabilities of the plant. Any cavern size beyond $1.2 \times 10^6$ $m^3$ offers only a small improvement to the plant's load following capabilities with a significant increase in cost and further restriction on available locations.

One further interesting observation that can be made from Figure 11 is that the integrated SOFC/CAES plant will be unable to provide perfect load following even with an infinitely large storage volume. This is since the maximum amplitude of weekly demand variation is too high for the CAES capacity to compensate for without the external use of atmospheric air (for charging) or the combustion of NG for pre-heating (for discharging). However, as a stand-alone plant meant to supply a demand profile with a moderate amplitude, it is conceivable that a SOFC/CAES system would be able to supply efficient power with nearly 100% reliability.

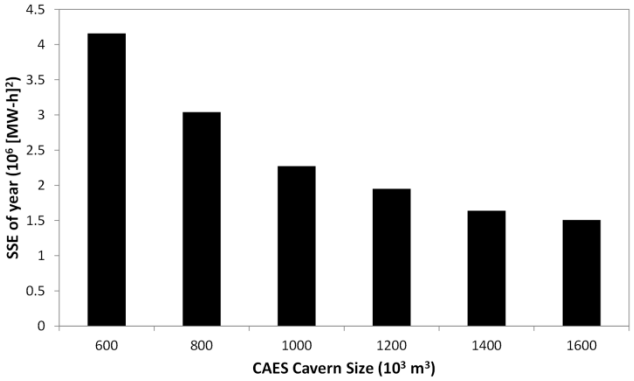


**Figure 11: SSE using the base case parameters for the two-level RHO scheme for various CAES storage volume sizes**

### *4.3. Pareto Trade-off Analysis Between Revenue and Load-Following Objectives*

A trade-off plot between the potential load-following and economic performance of the SOFC/CAES system using the proposed two-level RHO method for various values of $\psi$ is shown in Figure 12. Note that the base case CAES storage volume of 600,000 $m^3$ was used to generate this plot. It can immediately be seen that greedy algorithm (used in the original work demonstrating the applicability of an SOFC/CAES plant for load following) falls well below the Pareto frontier denoting the optimal achievable combinations of revenue generation and load following. In fact, using the proposed two layer RHO method offers both an increase in revenue (1.5%) and a reduction in SSE simultaneously. Alternatively, it is possible to choose $\psi$ to be a value between 0.75 and 0.90 in order to obtain approximately an increase in revenue of 6.5% ($14.6 million) relative to the base case study in this work with the same load-following performance. Any points beyond the Pareto front in Figure 12 is an infeasible operating condition based on the constraints of the CAES system when integrated with the SOFC power island. However, increases in storage

volume size, external air and heat sources, and lower demand profile amplitudes can push the frontier further upwards and to the left.

It is also interesting to note that a base-load only SOFC plant sized to the average demand for the year (720 MW) has an excessively high SSE and is thus not included on the Pareto front axes, clearly making it a sub optimal method of operation. Furthermore, such a plant would have to be sized to always meet the highest possible demand, which would be very wasteful from a resource consumption perspective.

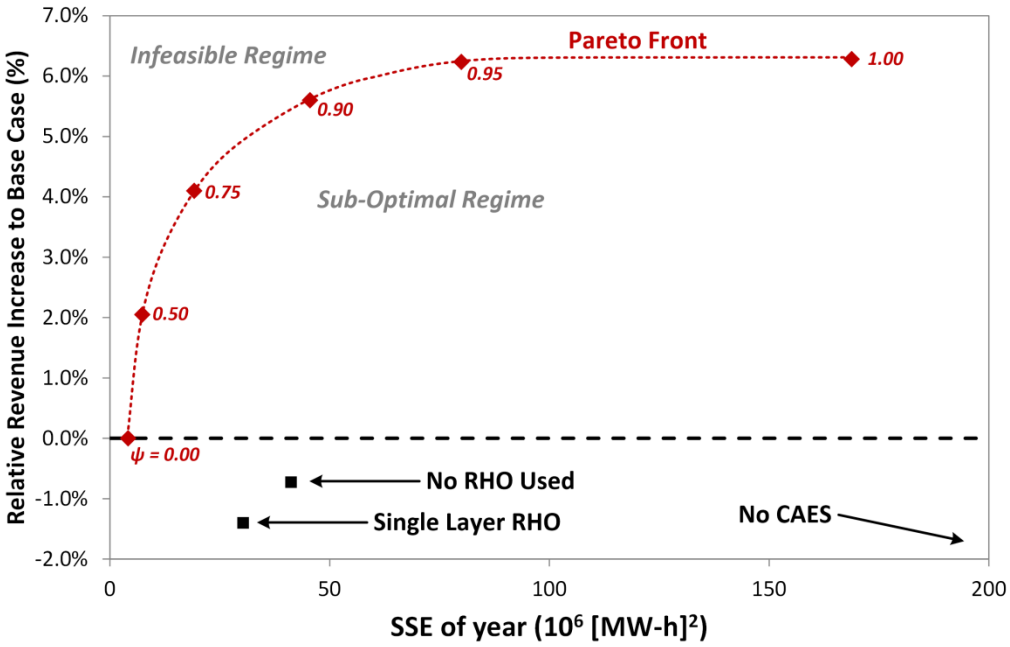


**Figure 12: Pareto frontier showing the trade-off between revenue generation and load-following capabilities of the SOFC/CAES plant for various values of $\psi$**

# 5. Conclusions and Recommendations

This study focused on the development of a two-stage RHO method that takes advantage of the hourly variability of CAES and the modular nature of SOFCs to provide reliable peaking power from an integrated SOFC/CAES plant with no $CO_2$ emissions. The first layer of the proposed RHO method used forecasted hourly demand to optimally operate the CAES portion of the integrated plant over the optimization time horizon (24 time steps were used in this case). The second layer of the RHO framework made adjustments to the SOFC baseload power island in order to adapt to seasonal drifts in demand throughout the year, a significant shortcoming of the single layer RHO previously proposed. The method was applied to a simulated SOFC/CAES plant fueled by coal designed in Aspen Plus v8.6. Simulations for one year of scaled demand data from the Province of Ontario, Canada were performed using a reduced-order model in MATLAB with all optimization calculations performed in GAMS using ANTIGONE and BARON. All simulation and control intervals were chosen to be one hour in order to use the demand data available. Since the impact of demand forecasting uncertainty was addressed in a prior work for individual weeks, this work focused on the performance of the plant when its baseload is selected optimally at the beginning of each week of operation.

It was found that the proposed two layer RHO method improved the load following performance of the SOFC/CAES plant by over 86% (from $30.3 \times 10^6$ to $4.15 \times 10^6$ [MW-h]$^2$) as measured by the SSE between demand and the power supplied by the plant for the 2014 year of operation. This is also a 90% improvement over the load-following capability of the integrated plant operating on an hour-by-hour basis (the so-called Greedy algorithm). It is worth noting that this improvement in demand/supply matching comes with no alterations to the plant design at all, but rather a more optimal utilization of the CAES peaking capabilities for hourly variations and the SOFC modularity to handle seasonal drifts in demand. Furthermore, it is possible to increase the revenue of the same plant by over $14 million (6.5%) per year if load following is not required via the tuning of the first-level objective function toward an economic focus. However, it should be noted that the proposed plant would require a larger SOFC power island (and hence capital investment), so a full techno economic trade-off analysis of the increased revenue should be the subject of a future work. A sensitivity analysis on the effect of CAES storage volume showed marked improvements in load following performance when more CAES storage is available, yielding a 53% improvement over the base case down to $1.95 \times 10^6$ (MW-h)$^2$. However, it was concluded that it would not be possible to completely eliminate supply/demand mismatches even with an infinitely large storage volume without significantly over-designing the power generation equipment.

Future work on this topic should include the investigation of uncertainty on the performance of the two stage RHO framework. Although prior studies found that demand forecast uncertainty did not significantly affect the hourly performance of the SOFC/CAES plant, it is possible that longer forecasts (and thus a greater degree of prediction error) could bias the second layer of the proposed technique and thus affect the baseload selection. Although it is not anticipated that this will significantly affect the results, it is something that should be addressed to test the robustness of this strategy to real-world noise and other sources of error.

Overall, the method showcased in this work has shown that, with the proper use of optimization strategies and by exploiting the advantages of the technologies therein, SOFC/CAES plants can be used to generate clean, reliable and efficient peaking power by using coal, which is a resource typically associated with the negative stigmas in all of these categories. The proposed RHO method overcomes the main weakness of the SOFC/CAES plant for peaking power by allowing it to slowly and safely adjust to seasonal changes in demand in an optimal manner, thereby more efficiently using the CAES system to save resources, money, and unnecessary wear on equipment. With these results, it is now apparent that technologies such as SOFCs and CAES are emerging as exciting opportunities that will permit the use of North America's abundant natural resources in a sustainable future for electricity production.

# 6. Acknowledgements

The authors would like to graciously acknowledge the Ontario Research Fund, the NSERC Vanier Canada Graduate Scholarship Program, and the Canada-Brazil Science Without Borders program for their financial support of this project.

# 7. Nomenclature

## *7.1. Abbreviations*

| | |
|---|---|
| CAES | Compressed Air Energy Storage |
| CCS | Carbon Capture and Sequestration |
| EOS | Equation of State |
| GT | Gas Turbine |
| HHV | Higher-Heating Value |
| HRSG | Heat Recovery and Steam Generation |
| IESO | Independent Electricity Systems Operator |
| RHO | Rolling Horizon Optimization |
| SOFC | Solid Oxide Fuel Cell |
| SSE | Sum of Squared Error |

## *7.2. Mathematical Symbols*

| | |
|---|---|
| $E$ | Power produced by SOFC/CAES plant (via optimization) |
| $\bar{E}$ | Actual power produced at each time step |
| $\dot{E}$ | initial guess for $E$ for proceeding simulation step |
| $P$ | Pressure in CAES storage (via optimization) |
| $\bar{P}$ | Actual pressure recorded in CAES storage at each time step |
| $\dot{P}$ | Initial guess for $P$ for proceeding simulation step |
| $n$ | Number of moles in CAES storage (via optimization) |
| $\bar{n}$ | Actual number of moles in cavern at each time step |

| | |
|---|---|
| $\dot{n}$ | Initial guess for $n$ for proceeding simulation step |
| $\mathcal{R}$ | Total revenue |
| $D$ | Demand |
| $F$ | Molar flow rate of cathode exhaust |
| $N$ | RHO forecasting horizon |
| $R$ | Universal gas constant |
| $V$ | Volume |
| $a$ | Model coefficient |
| $f(\cdots)$ | SOFC/CAES reduced model |
| $\delta$ | Binary charge/discharge decision variable |
| $\dot{\delta}$ | Initial guess for $\delta$ for proceeding simulation step |
| $\omega$ | Price of electricity |
| $\psi$ | User-defined economic/load-following weight factor |
| $\Phi$ | Economic/load-following objective function |
| $BL$ | Base load |
| $S$ | Cathode exhaust diversion parameter |
| $\mathcal{V}$ | Molar volume |
| $\Delta$ | Time step length |
| $a_{SRK}, b_{SRK}$ | SRK model coefficients |

### *7.3. Subscripts*

| | |
|---|---|
| $i$ | First-stage simulation/control time step |
| $\iota$ | Second-stage simulation/control time step |

| | |
|---|---|
| $t$ | First-stage RHO calculation time horizon step |
| $\tau$ | Second-stage RHO calculation time horizon step |
| $m$ | Reduced model identifier |
| $k$ | Reduced model variable identifier |
| $a, b, c$ | Reduced model order/coefficient identifiers |
| $max$ | Maximum allowable value |
| $min$ | Minimum allowable value |

# References


[1] US Energy Information Administration, Annual Energy Outlook 2014, US DOE/EIA-0383(2014). April 2014.

[2] National Energy Board. Canada's Energy Future: Energy Supply and Demand Projections to 2035 - Electricity Outlook Highlights. [online] Accessed June, 2012. [online]. Available HTTP: http://www.neb-one.gc.ca/clfnsi/rnrgynfmtn/nrgyrprt/nrgyftr/2011/fctsht1134lctrct-eng.html.

[3] D. Beevers, L. Branchini, V. Orlandini, A. De Pascale, H. Perez-Blanco. Pumped hydro storage plants with improved operational flexibility using constant speed Francis runners. *Applied Energy*. **2015**, *137*, 629-637.

[4] H. Sun, X. Luo, J. Wang. Feasibility study of a hybrid wind turbine system – Integration with compressed air energy storage. *Applied Energy*. **2015**, *137*, 617-628.

[5] A.k. Srivastava, J.Y. Kudariyawar, A. Borgohain, S.S. Jana, N.K. Maheshwari, P.K. Vijayan. Experimental and theoretical studies on the natural circulation behaviour of molten salt loop. *Applied Thermal Engineering*. **2016**, *98*, 513-521.

[6] G. Zanganeh, M. Commenford, A. Haselbacher, A. Pedretti, A. Steinfeld. Stabilization of the outflow temperature of a packed-bed thermal energy storage by combining rocks with phase change materials. *Applied Thermal Engineering*. **2014**, *70*, 316-320.

[7] BP Energy. BP Statistical Review of World Energy June 2014 (2014). Available HTTP: http://www.bp.com/content/dam/bp/pdf/Energy-economics/statistical-review-2014/BP-statistical-review-of-world-energy-2014-full report.pdf.

[8] T.A. Adams II, P.I. Barton. Systems and methods for the separation of carbon dioxide from water. US Patent App. 12/434486 (2009).

[9] EG&G Technical Services, DOE/NETL Fuel Cell Handbook, seventh ed., November 2004.

[10] M.C. Williams, J.P. Strakey, W.A. Surdoval. U.S. Department of Energy's solid oxide fuel cells: Technical advances. *International Journal of Applied Ceramic Technology.* **2005**, *2*, 295.

[11] J. Nease, T.A. Adams II. Coal-Fuelled Systems for Peaking Power with 100% $CO_2$ Capture Through Integration of Solid Oxide Fuel Cells with Compressed Air Energy Storage. *J. Power Sources*. **2014**, *251*, 92.

[12] N.Q. Ming. Coal based solid oxide fuel cell technology development. *ECS Transactions.* **2007**, *7*, 45.

[13] J. Nease, T.A. Adams II. Systems for peaking power with 100% $CO_2$ capture by integration of solid oxide fuel cells with compressed air energy storage. *J. Power Sources*. **2013**, *228*, 281.

[14] J. Nease, T.A. Adams II. Life Cycle Analyses of Bulk-Scale Solid Oxide Fuel Cell Power Plants and Comparisons to the Natural Gas Combined Cycle. *The Canadian Journal of Chemical Engineering*. **2015**, *93*, 1349-1363.

[15] J. Nease, T.A. Adams II. Comparative life cycle analyses of bulk-scale coal-fueled solid oxide fuel cell power plants. *Applied Energy*. **2015**, *150*, 161-175.

[16] B. Chachuat, B. Srinivasan, D. Bonvin. Adaptation strategies for real-time optimization. *Computers & Chemical Engineering*. **2009**, *33(10)*, 1557–1567.

[17] G. De Souza, D. Odloak, A.C. Zanin. Real time optimization (RTO) with model predictive control (MPC). *Computers & Chemical Engineering*. **2010**, *34(12)*, 1999–2006.

[18] A.C. Zanin, M. Tvrska de Gouvea, D. Odloak. Industrial implementation of a real-time optimization strategy for maximizing production of LPG in a FCC unit. *Computers & Chemical Engineering* **2010**, *24*m 525–531.

[19] C. Zhao, J. Fu, Q. Xu. Real-Time Dynamic Hoist Scheduling for Multistage Material Handling Process Under Uncertainties. *AICHE Journal*. **2013**, *59(2)*, 465–482.

[20] G.A. Bunin, Z. Wuillemin, G. Francois, A. Nakajo, L. Tsikonis, D. Bonvin. Experimental real-time optimization of a solid oxide fuel cell stack via constraint adaptation. *Energy*. **2012**, *39*, 54-62.

[21] J. Nease, T.A. Adams II. Application of rolling horizon optimization to an integrated solid oxide fuel cell and compressed air energy storage plant for zero-emissions peaking power under uncertainty. *Computers & Chemical Engineering*. **2014**, *68*, 203-219.

[22] T.A. Adams II, P.I. Barton. High-efficiency power production from coal with carbon capture. *AIChE Journal*. **2010**, *56*, 3120.

[23] GREET, The Greenhouse Gases, Regulated Emissions, and Energy Use In Transportation Model, GREET 1.8d.1, developed by Argonne National Laboratory, Argonne, IL, released August 26, 2010. Available HTTP: http://greet.es.anl.gov/.

[24] M.C. Woods, P.J. Capicotto, J.L. Haslbeck, N.J. Kuehn, M. Matuszewski, L.L. Pinkerton, M.D. Rutkowski, R.L. Schoff, V. Vaysman. Cost and Performance Baseline for Fossil Energy Plants. Volume 1: Bituminous Coal and Natural Gas to Electricity Final Report, DOE/NETL-2007/1281, Revision 1, August 2007.

[25] K. Krulla. Assesment of the Distributed Generation Market Potential for Solid Oxide Fuel Cells. United States Department of Energy – National Energy Technology Laboratory. SECA Conference proceeding. Pittsburgh, PA. July 23-24, 2013.

[26] S. D. Vora, Fuel Cells Program Overview. United States Department of Energy – National Energy Technology Laboratory. SECA Conference proceeding. Pittsburgh, PA. July 23-24, 2013.

[27] Fuel Cell Today, *The Fuel Cell Today Industry Review 2011*. September 14, 2011. Corporate report.

[28] T.A. Adams II, J. Nease, D. Tucker, P. Barton. Energy Conversion with Solid Oxide Fuel Cell Systems: A Review of Concepts and Outlooks for the Short- and Long-Term. *I&EC Research*. **2013**, *52(9)*, 3089-3111.

[29] F. Mueller, B. Tarroja, J. Maclay, F. Jabbari, J. Brouwer , S. Samuelson. Design, Simulation and Control of a 100 MW-Class Solid Oxide Fuel Cell Gas Turbine Hybrid System. *Journal of Fuel Cell Science and Technology*. **2010**, *7*, 031007-1-12.

[30] W.L. Luyben. Compressor heuristics for conceptual process design. *Industrial and Engineering Chemistry Research.* **2011**, *50*, 13984-13989.

[31] Raju M, Khaitan SK. Modeling and simulation of compressed air storage in caverns: A case study of the Huntorf plant. *Applied Energy.* 2012; 89:474-481.

[32] Rosenthal R. GAMS – A User's Guide. *GAMS Development Corporation.* Washington, DC, USA. 2012.

[33] Independent Electricity System Operator. *Ontario Demand and Market Prices*. Accessed March 19, 2012. Available HTTP: http://www.ieso.ca/imoweb/siteShared/demand_price.asp?sid =ic.

[34] Smith JM, Van Ness H, Abbot M. *Introduction to Chemical Engineering Thermodynamics – 7th Edition*. McGraw-Hill. New York, NY, United States. 2005.